Dynamics of complex interfaces

Raymond Kapral
Chemical Physics Theory Group, Department of Chemistry, University of Toronto, Toronto, Canada M5S 1A1

Roberto Livi
Dipartimento di Fisica, Università di Firenze, Istituto Nazionale di Fisica Nucleare and Istituto Nazionale de Fisica della Materia, Firenze, Italy

Gian-Luca Oppo
Department of Physics and Applied Physics, University of Strathclyde, Glasgow, G4 0NG, United Kingdom

Antonio Politi
Istituto Nazionale di Ottica and Istituto Nazionale di Fisica Nucleare, Firenze, Italy
(Received 7 October 1993)

Complex interfacial dynamics is studied in an oscillatory medium described by a deterministic coupled-map lattice. This dynamical system supports only stable periodic attractors. The interfaces that separate the stable homogeneous phases exhibit different types of behavior ranging from simple planar fronts with low periodicity to highly irregular fronts with complex spatiotemporal transients. A dynamical analysis of the system is carried out for a small interface length L, in which the probabilities of occurrence of given periodic orbits, the velocities of the corresponding interfaces, and Lyapunov exponents are calculated. The importance of transient dynamics for large L is demonstrated. In the large-L regime the interfacial evolution and structure are characterized in statistical terms and the simulation results are compared with phenomenological stochastic models such as the Edwards-Wilkinson and Kardar-Parisi-Zhang equations. In some parameter regions, the deterministic, transient interfacial dynamics of the coupled-map model is described well by such models if finite-size effects are taken into account. Nucleation and growth dynamics are also investigated. The system provides a framework in which to study complex interfacial structures.

PACS number(s): 05.40.+j, 05.45.+b, 47.20.Ky, 68.10.−m

I. INTRODUCTION

Interfaces separating two phases need not be simple and may exhibit varying degrees of spatial and temporal complexity. The structure and dynamics of such interfaces play an important role in a number of problems, including those related to the description of solidification fronts [1], diffusion-limited aggregation clusters [2], and chemical wave fronts [3]. When such complex interfaces occur they can give rise to phenomena that are not present in systems with smooth interfaces. Fingering instabilities and fractal growth processes are common examples. Often the gross aspects of such interfacial dynamics and structure can be captured by simple phenomenological models that incorporate the basic elements of the growth dynamics without reference to the detailed physics of a particular system. The well-known and often-studied Edwards-Wilkinson [4] and Kardar-Parisi-Zhang [5] equations are of this type.

In this article we consider oscillatory media which may also display complex front propagation and structure [6]. Rather than focusing on a specific physical system we consider a discrete dynamical model with oscillatory local elements. The simplicity of the model allows us to carry out a rather detailed study of the interfacial dynamics. Here the interface separates two phases of the oscillation. In spite of its simplicity this model system displays a bewildering variety of interfacial structures.

More specifically, the dynamical system studied is a deterministic, two-dimensional (2D) coupled-map lattice (CML). The discrete-time maps have the form

$$u' = f(u) = \begin{cases} bu & \text{for } u \le 1/b \\ a & \text{for } u > 1/b \end{cases}, \tag{1}$$

where $u \in (0,1)$. The map parameters a and b can be tuned to produce dynamics with any integer period n. The dynamics of an isolated map is extremely simple: all periodic orbits are superstable due to the existence of the map branch with zero slope, which must be visited by any orbit. The coupled-map lattice is

$$u(x,y,t+1) = (1-4\varepsilon) f(u(x,y,t)) + \varepsilon \sum_{(x,y)\in\mathcal{N}} f(u(x,y,t)), \tag{2}$$

where (x,y) are integer lattice-site labels, t is the discrete time, $\mathcal{N}$ is the Von Neumann neighborhood, and ε gauges the strength of the diffusive coupling. (In order for u to be confined to the unit interval ε is always smaller than 1/4.)

Since map (1) shows a simple dynamics and the coupling in (2) is purely diffusive, one might anticipate that the dynamics of the CML cannot exhibit chaotic proper-

ties. We shall show that while this is true for the asymptotic dynamics of the system, the transient dynamics is very complex indeed. For instance, in addition to the commonly encountered types of interfacial dynamics, we find that in certain parameter ranges waves may propagate in the system with velocities that depend on the diffusion constant in a nontrivial way, wave-front collision can give rise to nucleation processes that spawn other phases and the interfaces themselves may become unstable forming nuclei for other types of growth dynamics. Such features may lead to unusual phase competition and domain growth and entail a reexamination of nucleation and growth processes that takes into account the possibly complex interfacial dynamics.

In this investigation we consider a number of general aspects of interfacial structure and dynamics in the context of this model. By parameter variation we are able to obtain a wide variety of interfacial structures ranging from simple, strictly planar fronts to fronts with complicated structure and instabilities. As a result we are able to consider the applicability of the phenomenological models in various regimes and identify some of the reasons for their breakdown. While our dynamical system is deterministic and its attracting states are purely periodic, the interface often presents stochastic behavior. Thus our study addresses the broader question of measures of spatial complexity and the origin of statistical behavior in deterministic dynamical systems.

In Sec. II we present an overview of the interfacial structure that arises as the diffusive coupling among the oscillatory elements is varied. Section III contains a dynamical systems analysis of the attracting states for small interfacial lengths, as well as a study of the nature of the transients that lead to the periodic attractors. The detailed characterization of the planar, disordered interfaces that exist within a certain parameter range is the topic of Sec. IV. Various correlation functions and other indicators of interfacial structure are computed and compared with phenomenological models. The breakdown of these models for some values of the diffusion coupling is also studied in this section. Nucleation and domain growth processes are the subjects of Sec. V. The growth of a single disk-shaped nucleus of one phase in a "sea" of another phase is studied and the critical nucleus size is determined. The nucleation-growth dynamics is cast into the form of a first-passage-time problem. Once again, comparisons with phenomenological models for such growth processes are made. Section VI presents a sketch of some results on spiral dynamics and contains the conclusions of this study.

II. OVERVIEW OF INTERFACIAL DYNAMICS

Our study of interfacial structure and dynamics will be limited to the case where the map parameters are $a = 1/10$ and $b = 5/2$ and the isolated map has a period-three orbit: $u_1^* = a = A$, $u_2^* = ab = B$, and $u_3^* = ab^2 = C$. We have chosen to work with a stable period-three orbit since this is the shortest period allowing different relative stabilities between pairs of the various phases. In fact, period-two is rather special in that an interface AB is immediately mapped onto BA, i.e., they are perfectly symmetric. On the other hand, higher periods should have much in common with the period-three case where, since $AB \to BC \to CA \to AB$, there is no left-right symmetry [8]. Without loss of generality, we shall always refer in what follows to the interface between the homogeneous phases A and C.

We focus on interfaces separating two stable phases generated from initial conditions of the form

$$u(x,y) = \begin{cases} u_m^* & \text{if } -N/2 \le y \le -W/2 \\ \eta(x,y) & \text{if } -W/2 < y < W/2 \\ u_n^* & \text{if } W/2 \le y \le N/2, \end{cases} \tag{3}$$

where $x \in \{1,\dots,L\}$, $n,m \in \{1,2,3\}$, and η is a random number uniformly distributed on $(0,1)$. Here W is the width of the initially perturbed interfacial zone while L and N are the system lengths parallel and perpendicular to the interface, respectively. In the simulations we have used periodic boundary conditions along x ($x = 1,\dots,L$), i.e., parallel to the interface. Transverse to the interface, N is automatically adjusted at each time step so that the interface is entirely contained in a rectangle of size $L \times (N+1)$. In particular, the lattice region of interest is suitably shifted to follow the translational motion of the interface. The above algorithm to iterate the 2D coupled map lattice is essentially equivalent to using no-flux boundary conditions along the y direction in a sufficiently wide region. These boundary conditions ensure that the system has translational invariance along the interface and that only a single interface exists in the system. In the above procedure, the transversal width N varies in the course of the simulation in order to accommodate the interfacial zone. If the interface becomes very rough or thick the size of the simulation lattice may become large. Apart from the obvious case of growing interfaces, there is also the general case of stable interfaces separating regions which converge only asymptotically to the homogeneous phases (the spatial profile corresponding to a heteroclynic connection between two distinct fixed points). However, for our CML model this problem does not arise since the map is superstable [$f(u)$ is constant for $u > 1/b$], so that the interfacial region remains strictly finite (see Ref. [7] for the analytical discussion of the 1D case).

Before entering into a detailed examination of the nature of the interface for a particular range of ε values, it is useful to give a brief survey of the interfacial dynamics. Regions corresponding to significantly different behavior are observed as the coupling strength ε changes. For this overview (and throughout the paper unless stated otherwise) we select $W = 3$. This is the smallest value of the width that guarantees nontrivial evolution. In fact, initially thinner interfaces ($W = 1,2$) usually give rise only to stable interfaces of period-three, while larger W values lead to complex asymptotic dynamics similar to that for $W = 3$ [9]. The parameter L plays a more relevant role in that it controls the amplitude of transverse fluctuations. In the overview we have chosen $L = 1000$, while in the following sections the dependence of the dynamical

properties on L is investigated.

Snapshots of the interface are shown in Fig. 1 for several values of ε. The color coding is such that increasing u values from a to 1 correspond to increasing grey levels from white to black. An examination of the interfacial dynamics over the range $0.0 \leq \varepsilon \leq 0.25$ yields the following general picture of the interfacial structures.

(i) For $\varepsilon \leq 0.13$, the interface, after developing small-scale irregularities during a short, and almost L-independent transient, freezes in space and does not propagate.

(ii) When $0.13 \leq \varepsilon \leq 0.16$, the interface moves in such a way that phase C consumes phase A (the other dynamical configurations being obtained by cyclic permutations), i.e., with a positive velocity. For intermediate ε values, the interface exhibits also irregular fluctuations with a structure similar to that for $\varepsilon = 0.17$ described below [cf. the images in Fig. 1(c), which correspond, from top to bottom, to increasing times]. Near both ends of this interval the interface emits "gliders." These gliders

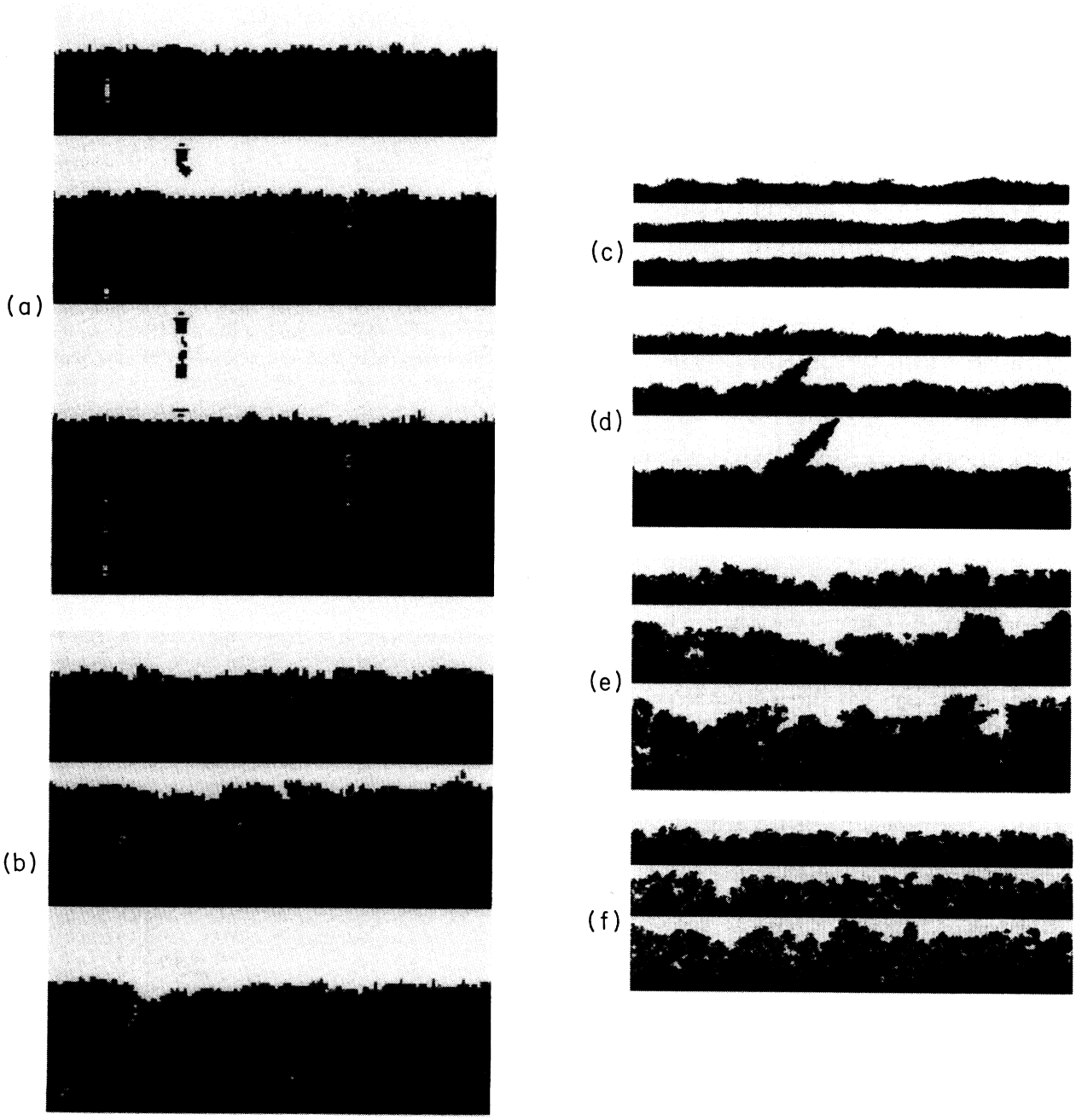

FIG. 1. Snapshots of the interface for various times. Time increases from the top frame to the bottom frame and y increases from the top to bottom of each frame. The time increment between frames is Δt. (a) Interface for $\varepsilon = 0.14$ emitting gliders perpendicular to the interface, $\Delta t = 60$; (b) interface emitting gliders at an angle to the interface for $\varepsilon = 0.16$, $\Delta t = 60$; (c) interface moving with negative velocity (A consumes C) for $\varepsilon = 0.17$, $\Delta t = 1200$; (d) interface develops deep fissures and long spikes for $\varepsilon = 0.188$, $\Delta t = 90$; (e) very rough interface that nucleates new homogeneous phases for $\varepsilon = 0.19$, $\Delta t = 300$; (f) interface becomes unstable and grows to consume the two stable phases for $\varepsilon = 0.193$, $\Delta t = 120$.

are isolated moving structures that detach from the interface and propagate into the otherwise homogeneous stable phases. They are similar to the gliders observed in some cellular automaton rules [10] [cf. Figs. 1(a) and 1(b). Note that only a portion of the $L = 1000$ interface is shown in these two figures in order to resolve the structures of the gliders].

(iii) For $0.16 \leq \varepsilon \leq 0.19$, the interface moves so that phase A consumes phase C (negative velocity) [cf. Fig. 1(c)]. The interfacial dynamics that occurs for $0.17 \leq \varepsilon \leq 0.18$ is of special interest in that the interface is rough and exhibits spatiotemporal complexity but is rarely fragmented. In this regime we investigate wave propagation and nucleation processes in a system where the interface itself exhibits nontrivial dynamics. When approaching the upper border of the interval, the interface develops various instabilities. For $\varepsilon = 0.188$, deep fissures arise and the third phase is nucleated during the evolution [Fig. 1(d)]. For $\varepsilon = 0.19$ the interface is very rough with breaking waves that produce "froth" which is sometimes absorbed by the stable phases but is also able to nucleate new phases [Fig. 1(e)].

(iv) When $\varepsilon > 0.19$ the interfacial region grows to consume the stable homogeneous phases. Eventually, the available space is filled by a single disordered phase [Fig. 1(f)].

III. DYNAMICAL SYSTEMS ANALYSIS

For small values of L the interfacial dynamics can be characterized in a rather complete way. In particular, it is possible to study a fairly large ensemble of different initial conditions and (i) determine the attractors eventually approached, (ii) estimate the length of the transient, and (iii) compute the velocity and Lyapunov exponents of the interface in each regime. For reasons of simplicity, our investigations have been restricted to the value $\varepsilon = 0.17$; however, similar results are expected to hold in a broad range of parameter values.

We have computed the probability $p_n(L)$ that an orbit of period n is eventually approached in a lattice of length L. The periodicity of the attractor was determined by monitoring the structure of the interface in the moving reference frame defined in Sec. II. In addition to the period, the average velocity of the interface is another important indicator allowing for a classification of the various attractors. The probability $p_n(L)$ was determined by averaging over 500 different realizations for increasing length L up to $L = 25$. The results for p_3 and p_6 are reported in Fig. 2 and show that the frequency of occurrence of period-three solutions falls rapidly to zero as L increases, while the probability of period-six interfaces increases towards unity. The periods of the remaining attractors are scattered over a very wide range (e.g., up to $n = 4800$ for $L = 24$) without any discernible pattern. There are a few period-three interfaces: all of them have a simple, strictly planar structure along the x direction, parallel to the interface. They can be described by a one-dimensional coupled map lattice. In contrast, period-six interfaces exhibit different transverse profiles, as do the

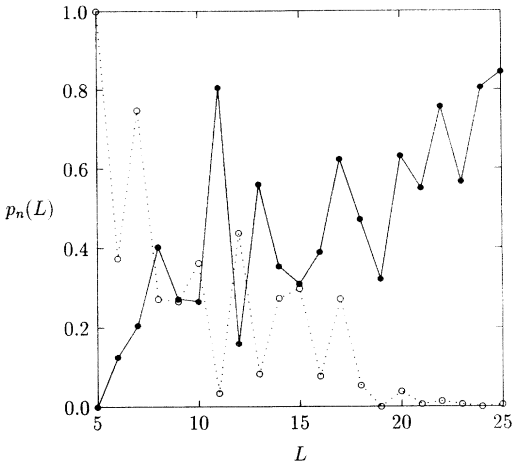

FIG. 2. Plot of $p_n(L)$, the probability of occurrence of period n in an interface of length L versus L for $n = 3$ (open circles) and $n = 6$ (closed circles).

interfaces with longer periods. This is consistent with the qualitative findings of Sec. II. For increasing L, the interface begins roughening during the transient, so that it becomes more and more unlikely that a planar structure will be approached eventually. In a few examples, gliders are periodically emitted by the interface thus preventing the convergence to a definite shape (mainly for $L = 10$, where 15% of the realizations do not appear to reach stable configurations of the interface).

Although it is obvious that all the attractors eventually reached are stable, it is not *a priori* obvious how their stability varies. A compact illustration of the various solutions found for $L \leq 25$ is provided in Fig. 3 where the maximum Lyapunov exponent λ is plotted versus the velocity of each periodic interface. A few cases are not represented in the figure since they fall outside the boundaries. They are (i) two period-three solutions characterized by a fairly large velocity ($v = -1/3$, $v = 1/3$) and (ii) a period-108 solution, characterized by $\lambda = -\infty$.

At this point it is interesting to observe that, despite

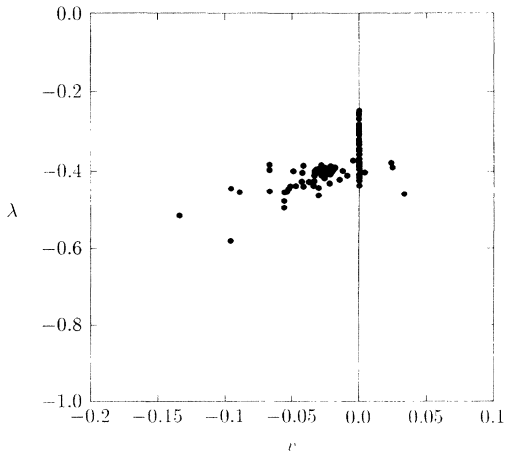

FIG. 3. Plot of the maximum Lyapunov exponent λ versus velocity v of the different periodic interfaces for $L \leq 25$.

the fact that the one-dimensional map $f(u)$ is superstable, superstable interfaces in the 2D lattice appear to be rather exceptional, again contradicting the common belief that diffusive coupling has a stabilizing effect. In this sense, we should also mention that an analytic study of the simplest stationary period-three solution (which is possible because of its strictly planar structure) shows that for values of ε such that $2\varepsilon^2 b^3(1-2\varepsilon) < 1$ even it becomes unstable to infinitesimal perturbations. Another interesting observation related to the results of Fig. 3 concerns the large number of stationary solutions. In particular, all the period-six interfaces are stationary, although characterized by different Lyapunov exponents.

Having described the possible asymptotic structures of the interface, we now wish to analyze the transient behavior preceding the collapse onto a periodic solution. This regime is typically characterized by an irregular evolution which is reminiscent of the 1D case studied in [11], where the initial condition was randomly chosen. Therefore, it is important to consider how the average length of the transient $\tau(L)$ scales with the length L. The average transient time needed to reach a periodic attractor using the same ensemble of realizations discussed above is reported in Fig. 4, where the logarithm of $\tau(L)$ is plotted versus $L^{3/2}$. The plot clearly shows that $\tau(L)$ increases faster than a simple exponential [namely, $\tau(L) \simeq \exp(0.079L^{3/2})$]. This scaling law is similar to that observed for the transients obtained in the one-dimensional version of this coupled map model, where a strictly exponential increase is found, and implies that all studies of the interfacial dynamics for large L ($L \geq 100$) are surely exploring the transient dynamics rather than the asymptotic attracting states. As noted in Refs. [12,11] it is this transient dynamics that is most relevant for systems of this type. The even faster growth observed in the present case is presumably due to the transversal structure of the interface. The longer the interface, the thicker it grows. Assuming that the transversal thickness is of the order $O(\sqrt{L})$ (see Sec. IV), the number of sites explored by the interface is of the order $O(L^{3/2})$. If, moreover, the evolution is characterized by short range correlations (again see Sec. IV), the probability of the collapse onto a periodic orbit is proportional to the simultaneous occurrence of $O(L^{3/2})$ almost independent events. This gives a heuristic explanation of the growth rate observed in the numerics of Fig. 4.

Finally, we have computed ensemble averages of both the velocity and the Lyapunov exponent for relatively short interfaces ($L = 20$). The velocity $v(t)$ was determined by computing the shift that occurred between the times $t-\Delta t$, $t+\Delta t$ ($\Delta t = 450$) and averaging over 10^5 different realizations. The effective Lyapunov exponent $\lambda(t)$ was determined in an analogous fashion by computing the contraction rate for the same time lag. The results shown in Fig. 5 reveal clearly the presence of two distinct regimes, both characterized by stationary properties, connected through a crossover region located at a time of the same order as the average transient reported in Fig. 4. Moreover, the "short time" plateaus exhibited by the velocity and the Lyapunov exponent coincide, within the numerical error, with the temporal averages computed for longer interfaces ($v = -0.0226$, $\lambda = -0.356$). Therefore, we claim that the transient is characterized by a

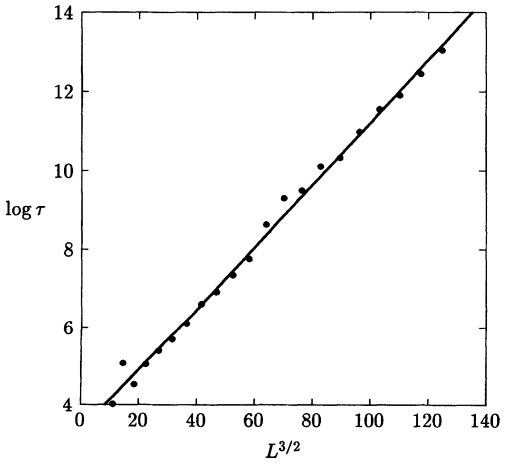

FIG. 4. Natural logarithm of the average transient time τ versus $L^{3/2}$. The solid circles are the simulation data and the straight line is a fit to the data: $\log\tau = 3.354 + 0.079L^{3/2}$.

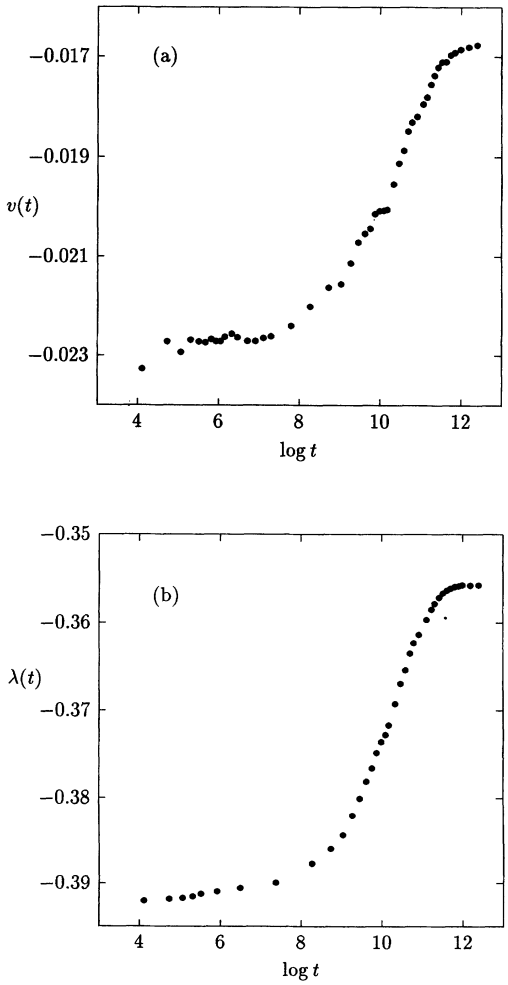

FIG. 5. (a) Effective velocity and (b) Lyapunov exponent versus the natural logarithm of the time for $L = 20$.

stationary, ergodic, length-independent dynamics. It is precisely this evolution that we shall analyze in the next section. We conclude by recalling that the "long time" regime, which appears stationary from Fig. 5, is nothing but the average over different attractors each characterized by its own velocity and stability.

IV. STATISTICAL MECHANICS OF THE INTERFACE

We shall use the term *disordered interface* when referring to interfaces with complex spatial structure such as those described above for the parameter range $0.17 \leq \varepsilon \leq 0.18$. The analysis in the following subsections will be restricted to the case study $\varepsilon = 0.17$, except for the last subsection where the dependence on the coupling parameter is considered. We compare the properties of our CML model with those of phenomenological, continuous models. To avoid proliferation of notation, the symbols x and t will be used to denote both the continuous and discrete space and time variables, respectively.

A. Structure and dynamics of the disordered interface

In this section we introduce the technical tools required to characterize the interfacial dynamics and discuss the results of the numerical simulations. The most important aspect of the dynamics is the evolution of the geometrical structure of the interface. A direct inspection [see, for instance, Fig. 1(c)] reveals that the two borders (profiles) of the interfacial region are described by regular curves which appear to be essentially single-valued functions of the lattice coordinate x (almost no overhangs are present).

We can define the interfacial border $h_C(x,t)$ $[h_A(x,t)]$ as the smallest [largest] y coordinate such that the dynamical variable $u(x,y,t)$ differs from the value of the homogeneous phase C (A) [13]. Given these definitions, the local interfacial thickness is $\Delta(x,t) = h_A(x,t) - h_C(x,t)$ and its mean value is given by

$$\bar{\Delta}(t) = \left\langle \frac{1}{L} \sum_{x=1}^{L} \Delta(x,t) \right\rangle , \tag{4}$$

where $\langle \cdot \rangle$ denotes average over independent realizations, and $\frac{1}{L}\sum \cdot$ is the space average. Numerical simulations show that $\bar{\Delta}(t) = 4.0$ with a standard deviation $\sigma_\Delta = 2.5$, almost independent of t and L. Such a small thickness implies that, for sufficiently large length scales, the interfacial region can be approximated by a 1D curve and, for practical purposes, described by either of the two borders. Henceforth we select $h_C(x,t)$ to be the profile and we denote by $h(x,t)$ its value measured in a reference frame where the center of mass of the profile is at rest (the subscript will be restored when referring specifically to one of the borders).

A natural description of the spatial structure of the profile is provided by the correlation function

$$C(x,t) = \left\langle \frac{1}{L} \sum_{x'=1}^{L} [h(x'+x,t) - h(x',t)]^2 \right\rangle . \tag{5}$$

A computation of this quantity was performed for $L = 200$, choosing the initial condition in (3) [i.e., $h(x, t = 0) = \text{const}$]. The results, reported in Fig. 6, show that correlations grow with time until an asymptotic parabolic curve is approached. The asymptotic form of the correlation function can be reproduced by assuming that the profile is a spatial Wiener process described by the diffusion equation [14]

$$\frac{\partial p(h,x|h_0,x_0)}{\partial x} = \mathcal{D} \frac{\partial^2 p(h,x|h_0,x_0)}{\partial h^2} \tag{6}$$

for the conditional probability $p(h,x|h_0,x_0)dh$ that the profile value is in $[h, h+dh]$ at site x, given the initial condition $h(x_0) = h_0$. Here $\mathcal{D}$ is a phenomenological diffusion coefficient. The solution of (6) is

$$p(h,x|h_0,x_0) = \frac{1}{\sqrt{4\pi\mathcal{D}(x-x_0)}} e^{-(h-h_0)^2/4\mathcal{D}(x-x_0)} . \tag{7}$$

In our case, in view of the periodic boundary conditions, we need to consider processes that return to h_0 after L steps. By including this constraint and setting, without loss of generality, $h_0 = 0$ and $x_0 = 0$, the resulting conditional probability density $P(h,x)$ is

$$P(h,x) = \frac{1}{\sqrt{4\pi\mathcal{D}x(L-x)/L}} e^{-h^2 L/4\mathcal{D}x(L-x)} . \tag{8}$$

The Wiener-process model for the correlation function $C_W(x)$ is then given by

$$C_W(x) = \int_{-\infty}^{\infty} dh h^2 P(h,x) = \frac{2\mathcal{D}}{L} x(L-x) . \tag{9}$$

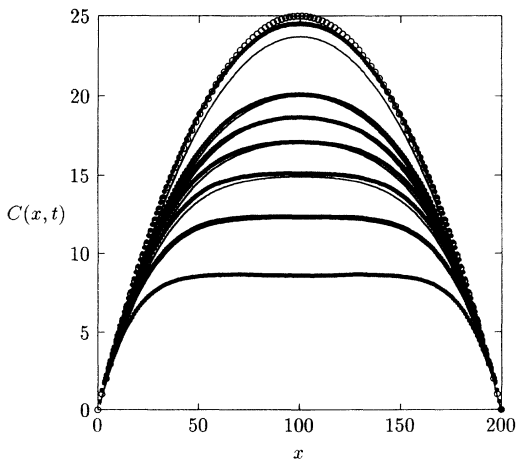

FIG. 6. Correlation function $C(x,t)$ versus x for $\varepsilon = 0.17$ at different times. The closed circles (which appear to be heavy solid lines) are the simulation data and the light lines are the theoretical curves obtained from the Edwards-Wilkinson model (27). Starting from bottom to top, the curves are for times $t = n \times 300$ with $n = 1, \ldots, 6$, while the topmost curve is for $t = 12 \times 300$. The open circles are the theoretical asymptotic value (28) of this correlation function.

By choosing $\mathcal{D} \sim 0.25$, the theoretical curve (9) reproduces the numerical data very well (cf. Fig. 6). This result indicates an unexpected stochastic behavior in space of our Lyapunov-stable deterministic CML system.

A further check of this simple stochastic model can be carried out by computing $P(h)$, the asymptotic probability distribution of interfacial heights, regardless of the value of the position along the interface,

$$P(h) = \frac{1}{L}\int_0^L dx P(h,x) \,. \tag{10}$$

Using the same value of $\mathcal{D}$ specified above, a comparison of this expression with the CML data is presented in Fig. 7; excellent agreement with the simulations is again obtained.

In order to gain further insight into the dynamics of the interface it is useful to analyze the evolution of the Fourier modes of the profile. We define the Fourier transform of $h(x,t)$ as

$$\hat{h}_k(t) = \frac{1}{L}\sum_{x=1}^{L} e^{ikx} h(x,t) \tag{11}$$

and let

$$M_k(t) = \langle |\hat{h}_k(t)|^2 \rangle \tag{12}$$

denote the average square amplitude of the kth Fourier mode. In view of the periodic boundary conditions we have $k = 2\pi n/L$ with $n = -L+1, \ldots, 0, \ldots, L-1$. In Fig. 8 we plot $k^2 L M_k(t)$ versus $k^2 t$ for several values of $k \neq 0$. The data for different modes lie on a single curve. This data collapse represents the starting point for the construction of a macroscopic model, discussed at length in Sec. IV B. The case $k = 0$ requires a separate analysis since, in contrast to the other mode amplitudes which eventually saturate, $M_0(t)$ grows linearly with time. This result indicates a temporal diffusive behavior which can be characterized by a second phenomenological diffusion

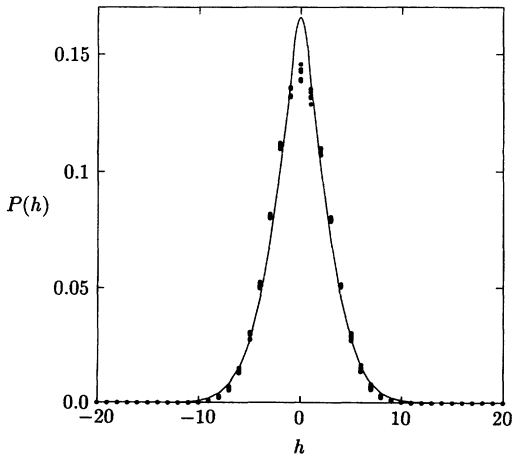

FIG. 7. Probability distribution $P(h)$ versus h for $\varepsilon = 0.17$. The solid circles are the simulation data for four different times while the solid line is the theoretical result obtained from (10).

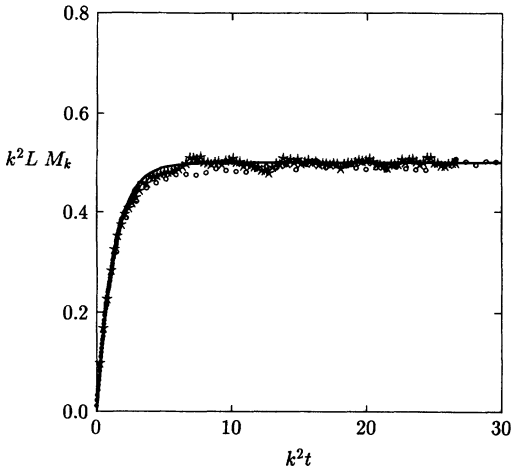

FIG. 8. Plots of $k^2 L M_k(t)$ versus $k^2 t$ for $\varepsilon = 0.17$. The different symbols refer to data for three values of the wave number k with indices $n = 1, 3, 5$. The solid line is the theoretical result from (22).

coefficient Γ; a fit of the numerical data gives $\Gamma = 0.2$.

Thus far, we have considered the geometrical properties of the interface, described as a 1D curve. There are at least two other quantities which characterize the interface: the state variable $u(x,y,t)$ along the profile and the thickness $\Delta(x,t)$. It is interesting to study their asymptotic spatial correlations.

The nature of correlations in the dynamical variable u in the interfacial region can be described in the following way. We let $\bar{u}(x,t)$ be the average value of $u(x,y,t)$ within the interfacial zone at position x and time t:

$$\bar{u}(x,t) = \Delta(x,t)^{-1} \sum_{y=h_C(x,t)}^{h_A(x,t)} u(x,y,t) \tag{13}$$

and define the correlation function of $\bar{u}$ as

$$C_I(x,t) = \frac{\left\langle \frac{1}{L}\sum_{x'=1}^{L} \delta\bar{u}(x'+x,t)\delta\bar{u}(x',t) \right\rangle}{\left\langle \frac{1}{L}\sum_{x=1}^{L} (\delta\bar{u}(x,t))^2 \right\rangle} \,, \tag{14}$$

where

$$\delta\bar{u}(x,t) = \bar{u}(x,t) - \left\langle \frac{1}{L}\sum_{x=1}^{L} \bar{u}(x,t) \right\rangle \,. \tag{15}$$

For increasing times, $C_I(x,t)$ rapidly converges to the asymptotic form plotted in Fig. 9. It is seen that correlations in $\bar{u}$ decay to zero in about seven lattice units.

In an analogous fashion, we define the spatial correlation function for the interfacial thickness $\Delta(x,t)$ as

$$C_\Delta(x,t) = \frac{\left\langle \frac{1}{L}\sum_{x'=1}^{L} \delta\Delta(x'+x,t)\delta\Delta(x',t) \right\rangle}{\left\langle \frac{1}{L}\sum_{x=1}^{L} [\delta\Delta(x,t)]^2 \right\rangle} \,, \tag{16}$$

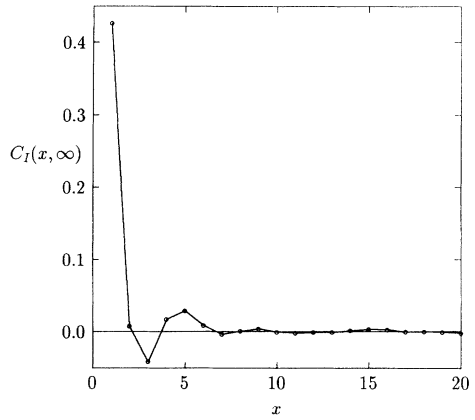

FIG. 9. Plot of the correlation function $C_I(x,\infty)$ versus x for $\varepsilon = 0.17$. Averages have been performed over 10^3 realizations.

where $\delta\Delta(x,t) = \Delta(x,t) - \bar{\Delta}(t)$. The results of a numerical computation of the asymptotic correlation function are reported in Fig. 10 and again show a fast decay of correlations (about ten lattice units).

All of these results obtained for a variety of different observables confirm that the interface behaves stochastically even over relatively short space and time scales. The construction of a coarse-grained model accounting for all of these features is a difficult task. In the following subsection, we limit ourselves to a comparison of the geometrical structure of the interfacial profile with known phenomenological models.

B. Macroscopic model

To model the complex deterministic dynamics of the interfacial profile, we suppose that $h(x,t)$ evolves in time due to three main mechanisms: (i) propagation with velocity v along the y direction, (ii) diffusion with an effective coefficient D along the x direction which acts like a surface-tension term that tends to remove surface roughness, and (iii) a random force accounting for the coupling with the remaining degrees of freedom [e.g., $u(x,y,t)$]. We stress that this noise term is self-generated and results from the nonlinear dynamics of the randomly initialized interface.

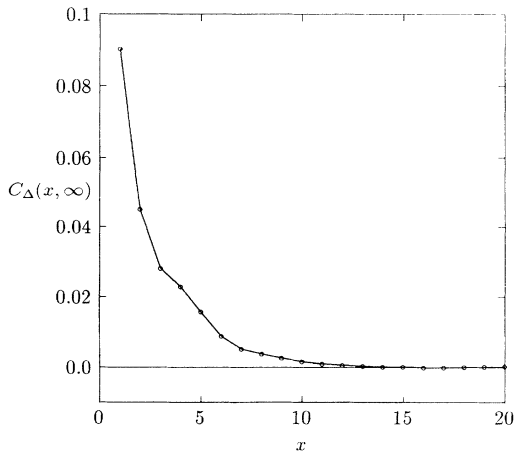

FIG. 10. Plot of $C_\Delta(x,\infty)$ versus x for $\varepsilon = 0.17$. Averages have been performed over 10^3 realizations.

The simplest equation which incorporates the above mechanisms and accounts for the scaling behavior reported in Fig. 8 is the Edwards-Wilkinson (EW) equation [4]

$$\frac{\partial h(x,t)}{\partial t} = D\frac{\partial^2 h(x,t)}{\partial x^2} + v + \xi(x,t) , \tag{17}$$

where v is the velocity of the interface. The noise term $\xi(x,t)$ is taken to be a Gaussian white-noise process with zero mean value and correlation function

$$\langle \xi(x,t)\xi(x',t')\rangle = 2\Gamma\delta(x-x')\delta(t-t') , \tag{18}$$

where for consistency Γ is the same coefficient introduced in Sec. IV A. If we make the replacement $h(x,t) \to h(x,t) + vt$, (17) becomes, in the moving reference frame,

$$\frac{\partial h(x,t)}{\partial t} = D\frac{\partial^2 h(x,t)}{\partial x^2} + \xi(x,t) . \tag{19}$$

This equation can be Fourier transformed defining

$$\hat{h}_k(t) = \frac{1}{L}\int_0^L dx e^{ikx} h(x,t) \tag{20}$$

and solved to give

$$\hat{h}_k(t) = e^{-Dk^2 t}\hat{h}_k(0) + \int_0^t dt' e^{-Dk^2(t-t')}\hat{\xi}_k(t') . \tag{21}$$

In view of the choice of the initial condition $h(x,0) = 0$, the expression for the square amplitude of the modes $M_k(t)$ is

$$M_k(t) = \frac{\Gamma}{Dk^2 L}\left(1 - e^{-2k^2 Dt}\right) . \tag{22}$$

This relation satisfies the general scaling ansatz made for rough interfaces [15]

$$M_k(t) \sim k^{-(1+2\alpha)}\mathcal{F}(tk^{\alpha/\beta}) \tag{23}$$

by fixing $\alpha = 1/2$ and $\beta = 1/4$, which are the known values for the EW model. The data collapse obtained in Fig. 8 can now be interpreted as the verification of this scaling behavior. Moreover, the two phenomenological parameters D and Γ can be extracted from the initial slope and the asymptotic value of $M_k(t)$,

$$\left(\frac{dM_k(t)}{dt}\right)_{t=0} = \frac{2\Gamma}{L} , \tag{24}$$

$$\lim_{t\to\infty} M_k(t) = \frac{\Gamma}{Dk^2 L} , \tag{25}$$

and we find $D = 0.4$ and $\Gamma = 0.2$. The theoretical expression (22) with these parameter values (solid line in Fig. 8) is in excellent agreement with the numerical data. Notice that the value of Γ coincides with the estimate obtained

in Sec. IV A from the evolution of $M_0(t)$.

The continuum version of the correlation function defined in (5)

$$C_{\rm EW}(x,t) = \frac{1}{L}\int_0^L dx'[\langle h(x',t)^2\rangle - \langle h(x'+x,t)h(x',t)\rangle] \tag{26}$$

may also be computed directly from (19). After substitution of the solution of (19) into this equation we find

$$C_{\rm EW}(x,t) = \sum_{n=1}^{\infty} \frac{4\Gamma L}{D(2\pi n)^2}\left[1-\cos(2\pi n x/L)\right] \times \left(1-e^{-2(2\pi n)^2 Dt/L^2}\right), \tag{27}$$

whose asymptotic value is

$$C_{\rm EW}(x) = \lim_{t\to\infty} C_{\rm EW}(x;t) = \frac{\Gamma}{LD}x(L-x)\,. \tag{28}$$

This expression is equivalent to (9) if one makes the identification

$$\mathcal{D} = \frac{\Gamma}{2D}. \tag{29}$$

Inserting the numerical values of Γ and D we recover the previous estimate of $\mathcal{D}$. To conclude this analysis, we have also compared the time-dependent expression (27) with our CML model, without any further fitting. The solid curves in Fig. 6 again agree very well with the numerical data.

Finally, for the sake of completeness, we have performed the analysis described in Sec. IV A for the lower border $h_A(x,t)$. If we still use the above-determined values of Γ and D, we find that the agreement with the numerical data has slightly deteriorated. For instance, the theoretical estimate $C_{\rm EW}(x,t)$ is systematically larger than the observed correlation $C(x,t)$. More precisely, the difference $\delta C(x,t) = C_{\rm EW}(x,t) - C(x,t)$ is nearly constant in space and time, except for small regions near $x = 0$ and $x = L$.

This is not a surprising result if one considers that $h_A(x,t) = h(x,t) + \Delta(x,t)$, so that the statistical properties of the lower border derive from the linear combination of an EW process and the thickness fluctuations of the interface. We have verified numerically that the autocorrelation of $\Delta(x,t)$ decays rapidly not only in space, but also in time and that the cross correlation of $\Delta(x,t)$ with $h(x,t)$ is negligible, so that $C(x,t) = C_{\rm EW}(x,t) + \sigma_\Delta^2$, a result consistent with the numerical findings. The different behavior exhibited by the two profiles stems from a nonzero velocity of the interface that breaks the symmetry between them. Accordingly, what is *a posteriori* surprising is that the upper profile $h_C(x,t)$ appears to be a pure EW process.

C. Finite-size effects

For increasing values of the coupling parameter ε in the interval (0.17, 0.18), a direct inspection of the interface borders shows the presence of an increasing number of overhangs. However, a quantitative analysis reveals that the density of overhangs per unit length remains so small (a few percent) that their effect can be neglected. Moreover, most of the features of the disordered interface discussed in Sec. IV A are still present. In particular, $\bar{\Delta}$ and $\sigma_{\bar{\Delta}}$ remain bounded to a few lattice units and $C_I(x,t)$ as well as $C_\Delta(x,t)$ decay rapidly to zero. As a consequence, one can maintain the previous definition of the interfacial profile and analyze its time evolution.

The square amplitudes $M_k(t)$ of the Fourier modes, plotted using the same scaling transformation adopted in Fig. 8, do not exhibit a good data collapse (see the case $\varepsilon = 0.175$ in Fig. 11). This disagreement with an EW-like behavior cannot be attributed to additional fluctuations of the interfacial thickness. In fact, the presence of such a stochastic contribution would lead to a spreading of the data in a direction opposite to that observed in Fig. 11. In view of this result one is led to consider more refined phenomenological models including nonlinear terms, and finite-size effects.

A widely used model that has been introduced to account for nonlinear contributions is the Kardar-Parisi-Zhang (KPZ) equation [5]

$$\frac{\partial h}{\partial t} = D\frac{\partial^2 h}{\partial x^2} + \frac{v}{2}\left(\frac{\partial h}{\partial x}\right)^2 + \xi(x,t)\,, \tag{30}$$

where $\xi(x,t)$ is the Gaussian process already defined in (18). This equation differs from the EW model in the moving reference frame only by the presence of the nonlinear term proportional to the velocity of the front.

We first discuss why these nonlinear corrections are irrelevant for $\varepsilon = 0.17$. According to the argument given in [16], one can estimate the critical length scale L_* above which the nonlinearity starts to play a relevant role as

$$L_* = \frac{152\,D^3}{v^2\Gamma}\,. \tag{31}$$

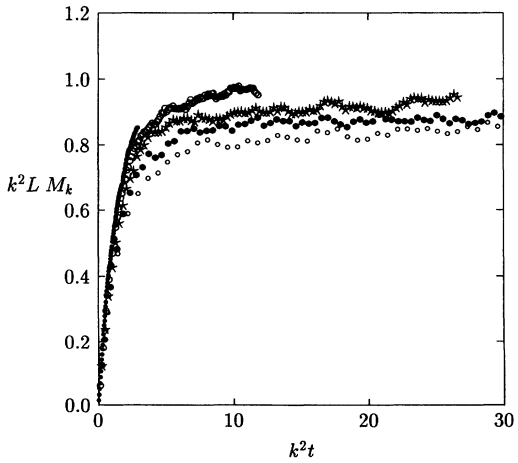

FIG. 11. Plots of $k^2LM_k(t)$ versus k^2t for $\varepsilon = 0.175$. The different symbols refer to data for five values of the wavenumber k with indices $n = 1,\ldots,5$.

Substituting the numerical values of the various parameters for $\varepsilon = 0.17$, we obtain $L_* \approx 80\,000$, a value much larger than the actual length of the interface chosen in the simulations ($L = 200$). If one could iterate sufficiently long interfaces, a crossover towards the behavior of the KPZ equation, characterized by the critical exponents $\alpha = 1/2$ and $\beta = 1/3$, should be observed; however, this is beyond the present numerical facilities.

A scaling analysis performed for $\varepsilon = 0.175$ [henceforth the analysis will be confined to this parameter value which typifies the behavior in the interval (0.17,0.18)] reveals that the estimates of α and β are still much closer to the EW values than to the ones of the KPZ equation. Given these results, it is reasonable to conjecture that the breakdown of the EW model, observed over the available length scales, can be explained in terms of finite-size corrections. In particular, this can be obtained by (i) adding higher-order derivatives in (19) or (ii) relaxing the δ-correlation assumption of the stochastic term. The leading correction from (i) is, on symmetry grounds, $\gamma_1 D \frac{\partial^4 h}{\partial x^4}$. The effect of this term can be described as a dependence of D on the wave number k in Fourier space [$D \to D(1 + \gamma_1 k^2)$]. The simplest way to take into account spatial correlations is to assume a Lorentzian profile for the power spectrum of the noise, i.e., $\Gamma \to \Gamma/(1 + \gamma_2 k^2)$ (this is equivalent to assuming a finite spatial correlation length $l_c = 2\pi\sqrt{\gamma_2}$).

The combined effect of these two hypotheses modifies (22) to

$$M_k(t) = \frac{\Gamma}{Dk^2 L(1+\gamma_1 k^2)(1+\gamma_2 k^2)} \times \left(1 - e^{-2k^2 D(1+\gamma_1 k^2)t}\right) . \quad (32)$$

A very good data collapse is obtained plotting $M_k(t)(1+\gamma_1 k^2)(1+\gamma_2 k^2)k^2$ versus $(1+\gamma_1 k^2)k^2 t$, for $\gamma_1 \simeq 0$ and $\gamma_2 \simeq 9$ (see Fig. 12). As a consequence it is sufficient to invoke a spatial correlation length l_c of about 19 lattice units in the (deterministically generated) noise term to account for the scaling behavior of the disordered interface. We can now evaluate the phenomenological parameters finding $\Gamma = 0.35$ and $D = 0.36$. The theoretical curve obtained for these values (solid line in Fig. 12) fits the data quite well.

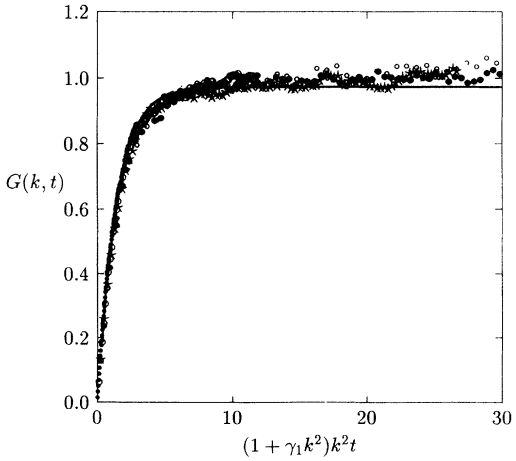

FIG. 12. Plots of $G(k,t) = M_k(t)(1+\gamma_1 k^2)(1+\gamma_2 k^2)k^2$ versus $(1+\gamma_1 k^2)k^2 t$ for $\varepsilon = 0.175$. The symbols are defined as in Fig. 11, while the solid line is the theoretical result from (32).

We are now in a position to determine the relevance of the KPZ nonlinear term. From (31), and considering that $v = -0.0386$, the critical length scale turns out to be $L_* \approx 7000$, that is, definitely shorter than for $\varepsilon = 0.17$, but still much larger than the length of the interface ($L = 200$).

Further numerical analyses show that the effect of nonlinear terms remains negligible for increasing ε, while finite-size corrections increase. This is consistent with the observation that a different dynamical phase is found when ε aproaches 0.19. Beyond this value fragmentation effects dominate the dynamics of the disordered interface, supporting the hypothesis of a dynamical phase transition to a different regime where the finite-size corrections become relevant over all length scales.

V. NUCLEATION AND GROWTH DYNAMICS

The planar interfacial geometry discussed above is the simplest context in which to carry out studies but, in general, curvature effects come into play and must be considered in order to obtain a more complete understanding of the system's dynamics. Most of the information concerning such effects can be obtained from a study of the dynamics of a single disk-shaped nucleus of a given homogeneous phase embedded in the sea of another homogeneous phase. More precisely, we study its growth rate and determine the critical radius for $\varepsilon = 0.17$ and 0.175. An general continuum model of the nucleation process is the polar-coordinate version of the KPZ equation. The corresponding stochastic differential equation is derived in the Appendix [see (A5)], starting from a general model written in a coordinate-independent representation [17]. In the Appendix, using the parameter values determined in Sec. IV, we also estimate the average size of angular fluctuations [see (A12)] which, for $\varepsilon = 0.17$ and 0.175, turn out to be very small. As a consequence the model,

$$\dot{\rho} = -\frac{D}{\rho} + v + \frac{\xi}{\sqrt{\rho}} \quad (33)$$

should be sufficient to describe the evolution of a single nucleus. Here ρ and ξ are the $n = 0$ components of the Fourier expansions in the angular degree of freedom of the interfacial profile and random force, respectively (cf. the Appendix).

Since a generic nucleus with initial radius ρ can either grow or collapse, it is useful to introduce the probability density $Q_f(\rho,t)$ for the stochastic process describing the nucleus dynamics to be absorbed at time t in $\rho_f > \rho$. This probability is known to satisfy the backward Kolmogorov equation [14]

$$\frac{\partial Q_f}{\partial t} = F(\rho)\frac{\partial Q_f}{\partial \rho} + \hat{\Gamma}(\rho)\frac{\partial^2 Q_f}{\partial \rho^2} , \quad (34)$$

where $F(\rho) = -D/\rho + v$ and $\hat{\Gamma}(\rho) = \Gamma/\pi\rho$. The normalization condition is

$$\int_0^\infty Q_f(\rho,t)dt = P_f(\rho)\ . \tag{35}$$

The probability $P_f(\rho)$ for the process to be eventually absorbed in ρ_f is given by [18]

$$P_f(\rho) = \int_0^\rho \frac{dr}{W(r)} \Big/ \int_0^{\rho_f} \frac{dr}{W(r)}\ , \tag{36}$$

where

$$W(r) = \exp\left[\int^r \frac{F(\rho)}{\hat{\Gamma}(\rho)}d\rho\right]\ . \tag{37}$$

The mean first-passage time is then defined by

$$T(\rho,\rho_f) = \frac{1}{P_f(\rho)}\int_0^\infty tQ_f(\rho,t)dt. \tag{38}$$

Multiplying (34) by t and integrating over t one obtains a differential equation for T:

$$F(\rho)\frac{\partial(TP_f)}{\partial\rho} + \hat{\Gamma}(\rho)\frac{\partial^2(TP_f)}{\rho^2} = -P_f\ . \tag{39}$$

By integrating (39) with the boundary conditions $T(\rho_f,\rho_f) = 0$, $T(0,\rho_f) < \infty$, one obtains (see [19] for a detailed discussion)

$$\begin{aligned} T(\rho,\rho_f) = &\int_\rho^{\rho_f} \frac{dr}{W(r)}\int^r \frac{P_f(r')W(r')}{\hat{\Gamma}(r')}dr' \\ &- \left(1 - \frac{1}{P_f(\rho)}\right) \\ &\times \int_0^\rho \frac{dr}{W(r)}\int^r \frac{P_f(r')W(r')}{\hat{\Gamma}(r')}dr'\ . \end{aligned} \tag{40}$$

Using these tools we are now in the position to compare the stochastic model with the CML dynamics. Before entering into the details of this comparison, we first consider the dependence of the velocity of the planar interface on its orientation with respect to the lattice. The maximum deviation is expected for an orientation $\pm\pi/4$ in which case we find $v = -0.0201$ and -0.0382 for $\varepsilon = 0.17$ and 0.175, respectively. Both values are close to the velocities estimated in Sec. IV ($v = -0.0226$ and -0.0386), although slightly smaller. Thus an isotropic model such as that described above should be able to provide a good representation of the observed evolution.

In analogy with the planar case, the randomly initialized interface is chosen to be an annulus with an external radius r_0 and a thickness corresponding to three lattice units. Phase A covers the disk interior to the annulus, which is surrounded by phase C. Snapshots of the evolution for one realization of the disk growth are shown in Fig. 13 for $\varepsilon = 0.17$. One can see that the disk deforms as it grows, although its shape remains circular on average. In this figure one may also observe that the interface itself exhibits a structure considerably more complex than that seen in the planar geometry discussed in Sec. IV for this parameter value. Thus the curvature for small radii induces additional interfacial structure.

In order to perform a quantitative analysis, the interfacial profile $\mathbf{r}(s,t)$ is defined as the border of phase C. Here s parametrizes the profile. Due to the fluctuations

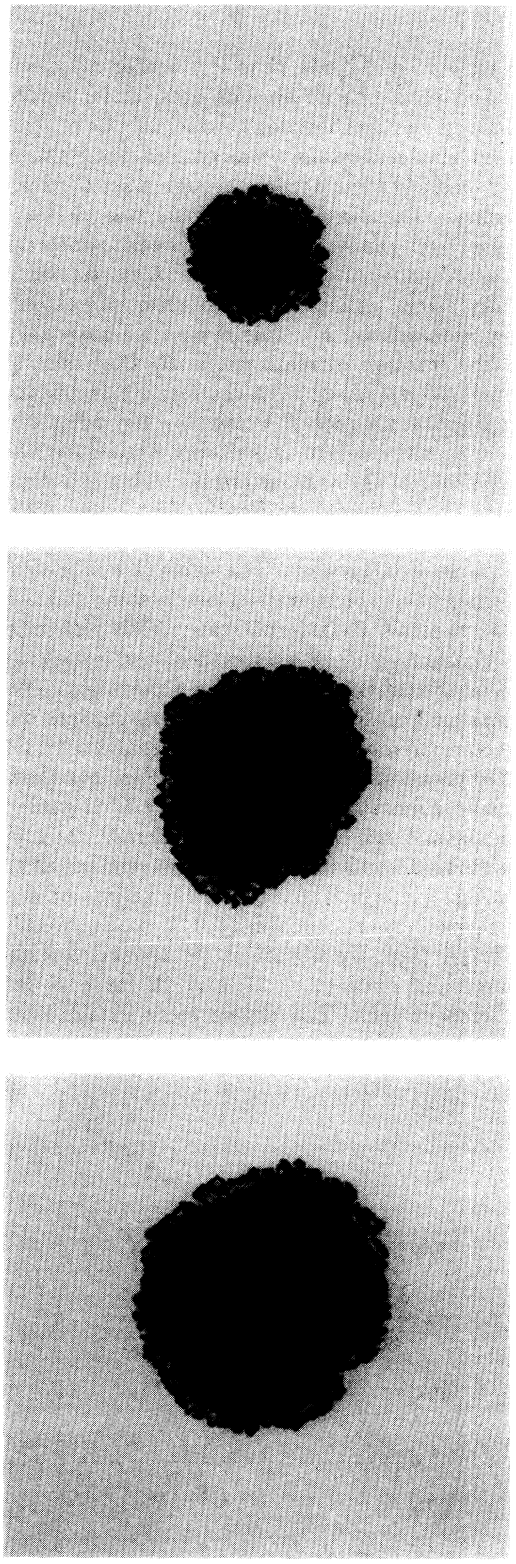

FIG. 13. Snapshots of the growth of a nucleus for $\varepsilon = 0.17$ for three times between $t = 90$ and $t = 3600$.

of the disordered interface it is useful to introduce the mean radius

$$\bar{\rho}(t) = \frac{1}{N_s} \sum_s |\mathbf{r}(s,t) - \mathbf{c}(t)| \,, \tag{41}$$

where $\mathbf{c}(t) = \frac{1}{N_s} \sum_s \mathbf{r}(s,t)$ is the center of mass of the profile and N_s is the number of sites in the profile.

Following the methodology sketched above, the study of the interfacial dynamics was carried out by measuring the first-passage time of $\bar{\rho}(t)$ through a set of preassigned thresholds. The statistical analysis was performed by averaging over many independent realizations with the same initial value of the radius r_0. A particular realization may either collapse to zero after some finite time or grow indefinitely. For this reason we have also determined the fraction of realizations P_f that pass through the threshold ρ_f, along with the mean first-passage time T. In Fig. 14 we plot T versus ρ_f for different values of r_0. The time origin is suitably chosen to show the superposition of the various curves. This is a direct confirmation that a single, stochastic, first-order, differential equation is sufficient to describe the dynamical behavior of the nucleation process. The same is not true at early times since each configuration needs some finite time to reach a "typical" disordered state. This relaxation process is characterized by a growth of the initial radius r_0 by two lattice units in the first few time steps. The corresponding part of the curves has been discarded in Fig. 14.

The comparison of the numerical results with the theoretical expression (40) (solid lines in Fig. 14) shows good agreement almost everywhere for $\varepsilon = 0.17$, while significant deviations are observed at small radii for $\varepsilon = 0.175$. This is further confirmed from measurements of the critical radius r_c defined as the initial radius of a nucleus characterized by a probability 1/2 to eventually grow [20]. From (36), we obtain $r_c \simeq 18$ and 9 while from the numerical data $r_c \simeq 19$ and 12 for $\varepsilon = 0.17$ and 0.175, respectively. The disgreement in the latter case cannot be explained by invoking strong finite-size corrections which would be inconsistent with the results found for the planar interface. Therefore, the observed disgreement can only originate from effects due to the finiteness of the lattice spacing.

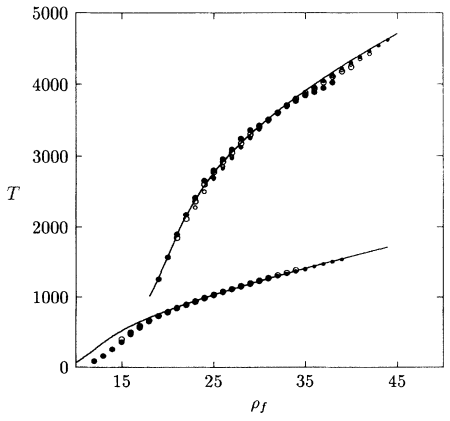

FIG. 14. T versus ρ_f for $\varepsilon = 0.17$ (a) and 0.175 (b) for different values of r_0. The time origins for the various cases are suitably translated to superpose the data. The theoretical results obtained from (40) are shown as solid lines.

VI. CONCLUSIONS AND PERSPECTIVES

We have demonstrated in this study that simple, deterministic, spatially extended systems whose attractors are strictly periodic can exhibit complex, long-lived transients with interesting interfacial structure which is stochastic in nature. The transient regime depends superexponentially on the system length L and thus it is the transient dynamics that is most relevant for all but the smallest system sizes. The interfacial dynamics of this transient regime can be characterized and modeled by simple *stochastic* equations, indicating that the deterministic nonlinear dynamics is able to mimic the effects of noise.

The interfacial dynamics is very rich and models of this type can serve as paradigms for the study of complex interfaces with structures reminiscent of those that arise in physical systems through different mechanisms. The CML model can serve as a testing ground for phenomenological models of interfacial dynamics whose form is based on general physical elements rather than details of a specific system. The investigations presented in this paper constitute a beginning of research in this direction.

The work presented above focused on the interface between two phases in both the planar and disk geometries. Studies of this type constitute an important element in the understanding of oscillatory media; however, even in our simple system with period-three local maps, one must in general consider the competition among three phases. We noted above that in certain parameter regimes the instabilities in the interface separating two phases can give rise to the nucleation of the third phase. In fact, starting from random initial conditions, the generic state of the system will consist of a competition among patches of the three phases, each consuming the other [8]. Three-phase coexistence implies the existence of point defects where all three phases meet. Such defects can serve as the source of spiral waves, which in some circumstances may break up to yield new defects. An example of spiral wave evolution and breakup in our model for $\varepsilon = 0.18$ is shown in Fig. 15. Stable spiral waves are obtained for $\varepsilon = 0.17$. Defect creation and destruction processes of this type may give rise to defect-mediated turbulence, a common scenario for spatiotemporal chaos in oscillatory media [21]. Our CML model can be used to study such chaotic states in a simpler context than the commonly employed complex Ginzburg-Landau models.

Finally, we stress that many aspects of the complex interfacial dynamics exhibited by this coupled-map model remain to be investigated, for example, the nature of the instability giving rise to the glider phases and the characterization of the interfacial thickness growth that leads to the ultimate destruction of the interface for large ε.

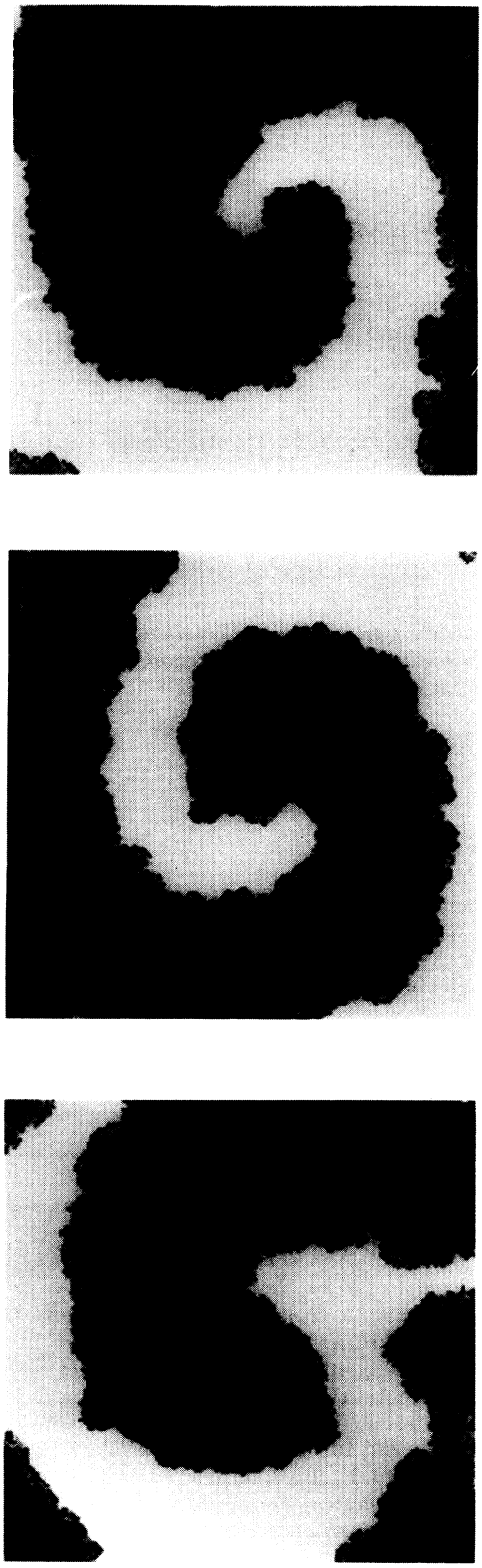

FIG. 15. Spiral wave dynamics and breakup initiated by the existence of a point defect where all three phases meet. The simulations were carried out on a 200×200 lattice with no-flux boundary conditions for $\varepsilon = 0.18$. From top to bottom, the frames are for $t = 2700$, $t = 3600$, and $t = 4500$, respectively.

ACKNOWLEDGMENTS

We are all grateful to ISI in Torino for the program on Complexity and Chaos which made possible the initial substantial progress on this research topic. The research of R.K. was supported in part by a grant from the Natural Sciences and Engineering Research Council of Canada. R.K. is also grateful to the Theoretical Physics FORUM of INFM which supported his stay in Firenze. G-L.O. acknowledges partial support from SERC and EEC/Esprit (TONICS). R.L. and A.P. thank also CPT of CNRS in Luminy for its hospitality.

APPENDIX

A general phenomenological description of interfacial dynamics that accounts for nonlinear contributions and overhangs has been proposed recently in Ref. [17]. The interface $\mathbf{r}(s,t) \equiv (x(s,t), y(s,t))$, parametrized by the continuous variable s, is assumed to satisfy the equation

$$\frac{\partial \mathbf{r}(s)}{\partial t} = D g^{-1/2} \frac{\partial}{\partial s} g^{-1/2} \frac{\partial}{\partial s} \mathbf{r}(s) + v\hat{n} + \eta \,, \qquad \text{(A1)}$$

where $g = |d\mathbf{r}/ds|^2$ and the correlation function of the random force η is

$$\langle \eta_\alpha(s,t) \eta_\beta(s',t') \rangle = 2\Gamma \delta_{\alpha\beta} g^{-1/2} \delta(s-s') \delta(t-t') \,. \qquad \text{(A2)}$$

This choice of the correlation guarantees that (A1) is independent of the parametrization adopted. In [17], it was shown that, in the no-overhang approximation and to first order in the nonlinear corrections, (A1) reduces to the KPZ equation (30).

In order to study the nucleation problem it is useful to refer to a polar coordinate system $x(s,t) = \rho(s,t)\cos\theta(s,t)$ and $y(s,t) = \rho(s,t)\sin\theta(s,t)$. In this representation, $g = \rho_s^2 + \rho^2 \theta_s^2$, where the subscript s indicates differentiation with respect to this variable. Assuming in (A1) that there are no overhangs, i.e., $\rho(s,t) = \rho(\theta,t)$, a straightforward but lengthy calculation yields

$$\begin{aligned} \frac{\partial \rho(\theta,t)}{\partial t} = {} & D \frac{1}{\sqrt{\rho_\theta^2 + \rho^2}} \frac{\partial}{\partial \theta} \frac{1}{\sqrt{\rho_\theta^2 + \rho^2}} \frac{\partial}{\partial \theta} \rho(\theta,t) \\ & - \frac{D}{\rho} \left(1 + \frac{\rho_\theta^2 (\rho_\theta^2 - \rho \rho_{\theta\theta})}{(\rho_\theta^2 + \rho^2)^2} \right) \\ & + \frac{v}{\rho} \sqrt{\rho_\theta^2 + \rho^2} + \frac{(\rho_\theta^2 + \rho^2)^{1/4}}{\rho} \xi(\theta,t) \,, \end{aligned} \qquad \text{(A3)}$$

where the random force term has correlation function

$$\langle \xi(\theta,t) \xi(\theta',t') \rangle = 2\Gamma \delta(\theta - \theta') \delta(t-t') \,. \qquad \text{(A4)}$$

If we further assume $\rho_\theta / \rho \ll 1$, we obtain the analog of the KPZ equation for the disk growth problem:

$$\frac{\partial \rho}{\partial t} = \frac{D}{\rho^2} \frac{\partial^2 \rho}{\partial \theta^2} - \frac{D}{\rho} + v \left(1 + \frac{\rho_\theta^2}{2\rho^2} \right) + \frac{1}{\sqrt{\rho}} \xi(\theta,t) \,. \qquad \text{(A5)}$$

Even neglecting the KPZ-like term, (A5) remains intrin-

sically nonlinear and the Fourier analysis cannot lead to an exact solution as for the EW model. Nevertheless, one can still extract information on the angular fluctuations by means of a perturbative analysis. By substituting

$$\rho(\theta,t)=\sum_{n=-\infty}^{+\infty}\rho_n(t)e^{in\theta} \tag{A6}$$

and

$$\xi(\theta,t)=\sum_{n=-\infty}^{+\infty}\xi_n(t)e^{in\theta} \tag{A7}$$

in (A5) with $\langle\xi_n(t)\xi_n(t')\rangle=\frac{\Gamma}{\pi}\delta(t-t')$ and multiplying both sides by ρ^2, one can formally obtain a hierarchy of stochastic differential equations. This set of equations refers to a fixed reference frame; however, in the study of the nucleation process it is necessary to determine the radial variable with respect to the actual position of the center of mass. The choice of such a reference frame amounts to setting $\rho_1(t)=\text{const}=0$. Accordingly, the leading corrections to $\rho_0(t)$ originate from $\rho_{\pm2}(t)$. In this perspective one can truncate the hierarchy of equations at $n=\pm2$. Keeping only the leading terms in the equations for $\rho_0(t)$, $\rho_{\pm2}(t)$, we obtain

$$\begin{aligned}&\rho_0^2\dot{\rho}_0+2\rho_2\rho_{-2}\dot{\rho}_0+2\rho_2\rho_0\dot{\rho}_{-2}+2\rho_{-2}\rho_0\dot{\rho}_2\\&\quad=-D\rho_0+v(\rho_0^2+6\rho_2\rho_{-2})\\&\qquad+\rho_0^{3/2}\left(\xi_0+\frac{3}{2}\frac{\rho_2}{\rho_0}\xi_{-2}\frac{3}{2}\frac{\rho_{-2}}{\rho_0}\xi_2\frac{3}{8}\frac{\rho_2\rho_{-2}}{\rho_0^2}\xi_0\right)\end{aligned} \tag{A8}$$

and

$$\rho_0^2\dot{\rho}_{\pm2}+2\rho_{\pm2}\rho_0\dot{\rho}_0=-5D\rho_{\pm2}+2v\rho_0\rho_{\pm2}+\rho_0^{3/2}\xi_{\pm2}\,. \tag{A9}$$

By neglecting any angular dependence (i.e., the dependence on $\xi_{\pm2}$ and $\rho_{\pm2}$), (A8) reduces to

$$\dot{\rho}_0=-\frac{D}{\rho_0}+v+\frac{\xi_0}{\sqrt{\rho_0}}\,, \tag{A10}$$

which gives the zeroth-order estimate for the critical radius $r_c=D/v$.

By substituting (A10) in (A9) and neglecting higher-order terms, we obtain

$$\dot{\rho}_{\pm2}=-3D\frac{\rho_{\pm2}}{\rho_0^2}+\frac{\xi_{\pm2}}{\sqrt{\rho_0}}\,. \tag{A11}$$

By substituting $\rho_0=r_c$ in this equation, one can estimate from the resulting Langevin equation the relative size of the angular fluctuations:

$$\frac{\langle\rho_{\pm2}^2\rangle}{r_c^2}=\frac{\Gamma v}{3\pi D^2}\,. \tag{A12}$$

[1] J.S. Langer, Rev. Mod. Phys. **52**, 1 (1980).

[2] *On Growth and Form*, edited by H.E. Stanley and N. Ostrowsky (Martinus Nijhoff Publishers, Dordrecht, 1986); *Kinetics of Aggregration and Gelation*, edited by F. Family and D.P. Landau (North-Holland, Amsterdam, 1984); *The Fractal Approach to Heterogeneous Chemistry*, edited by D. Avnir (Wiley, New York, 1989).

[3] *Oscillations and Traveling Waves in Chemical Systems*, edited by R.J. Field and M. Burger (Wiley, New York, 1985).

[4] S.F. Edwards and D.R. Wilkinson, Proc. R. Soc. London Ser. A **381**, 17 (1982).

[5] M. Kardar, G. Parisi, and Y.-C. Zhang, Phys. Rev. Lett. **56**, 889 (1986).

[6] See, for instance, M.C. Cross and P.C. Hohenberg, Rev. Mod. Phys. **65**, 851 (1993).

[7] L.A. Bunimovich, R. Livi, G. Martinez-Mekler, and S. Ruffo, Chaos **2**, 283 (1992)

[8] C.H. Bennett, G. Grinstein, Y. He, C. Jayaprakash, and D. Mukamel, Phys. Rev. A **41**, 1932 (1990).

[9] If W is sufficiently large, nucleation of the third phase in the interfacial zone may occur with high probability.

[10] *Dynamical Systems and Cellular Automata*, edited by J. Demongeot, E. Golès, and M. Tchuente (Academic, New York, 1985).

[11] A. Politi, R. Livi, G.-L. Oppo, and R. Kapral, Europhys. Lett. **22**, 571 (1993)

[12] J.P. Crutchfield and K. Kaneko, Phys. Rev. Lett. **60**, 2715 (1988).

[13] This definition of the border is unambiguous because of the superstability of map (1), which ensures a collapse onto the value of the homogeneous phase after a finite number of steps.

[14] C.W. Gardiner, *Handbook of Stochastic Processes* (Springer-Verlag, New York, 1985).

[15] S.V. Buldyrev, A. L. Barábasi, F. Caserta, S. Havlin, H.E. Stanley, T. Vicsek, and V.S. L'vov, Phys. Rev. A **45**, R8313 (1992).

[16] K. Sneppen, J. Krug, M.H. Jensen, C. Jayaprakash, and T. Bohr, Phys Rev. A **46**, R7351 (1992)

[17] A. Maritan, F. Toigo, J. Koplik, and J. Banavar, Phys. Rev. Lett. **69**, 3193 (1992).

[18] W. Feller, *An Introduction to Probability Theory and its Applications* (Wiley, New York, 1966), Vol. 2.

[19] F.T. Arecchi, A. Politi, and L. Ulivi, Nuovo Cimento **71B**, 119 (1982).

[20] The initial condition used to define r_c is not r_0, but it is measured after the initial relaxation process dies out.

[21] See, for instance, P. Coullet, L. Gil, and J. Lega, Phys. Rev. Lett. **62**, 161 (989); T. Bohr, A.W. Pedersen, M.H. Jensen, and A.D. Rand, in *New Trends in Nonlinear Dynamics and Pattern Forming Phenomena: The Geometry of Nonequilibrium*, edited by P. Coullet and P. Huerre (Plenum, New York, 1989); G. Huber, P. Alstrom, and T. Bohr, Phys. Rev. Lett. **69**, 2380 (1992).

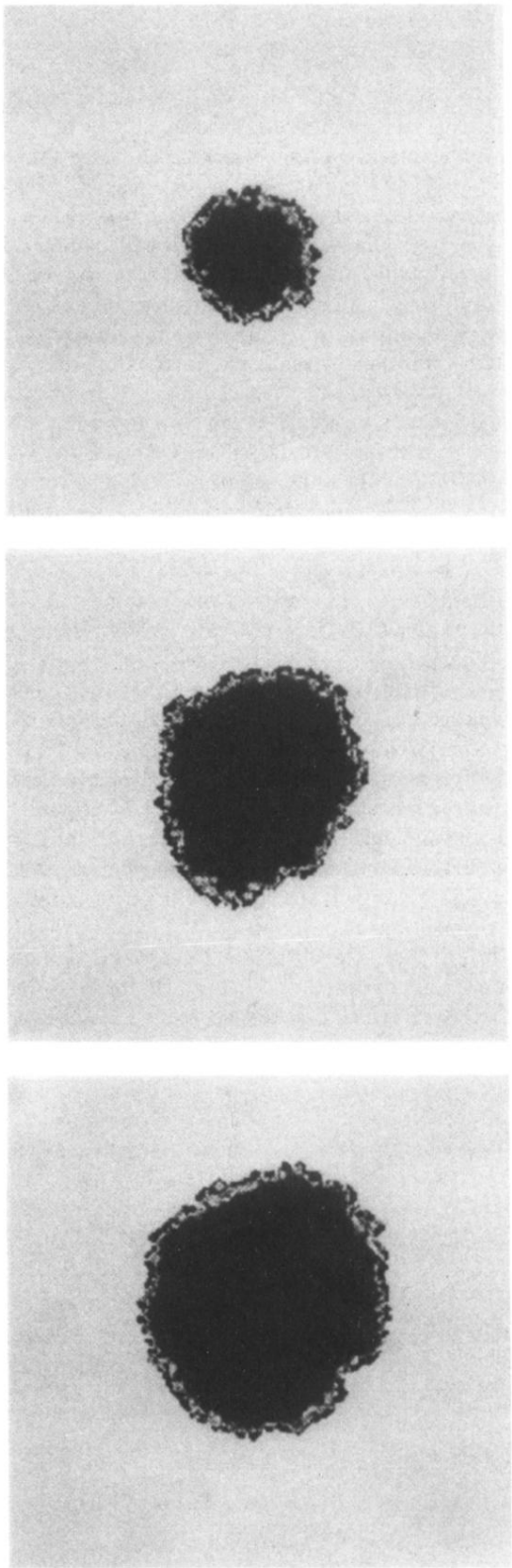

FIG. 13. Snapshots of the growth of a nucleus for $\epsilon = 0.17$ for three times between $t = 90$ and $t = 3600$.

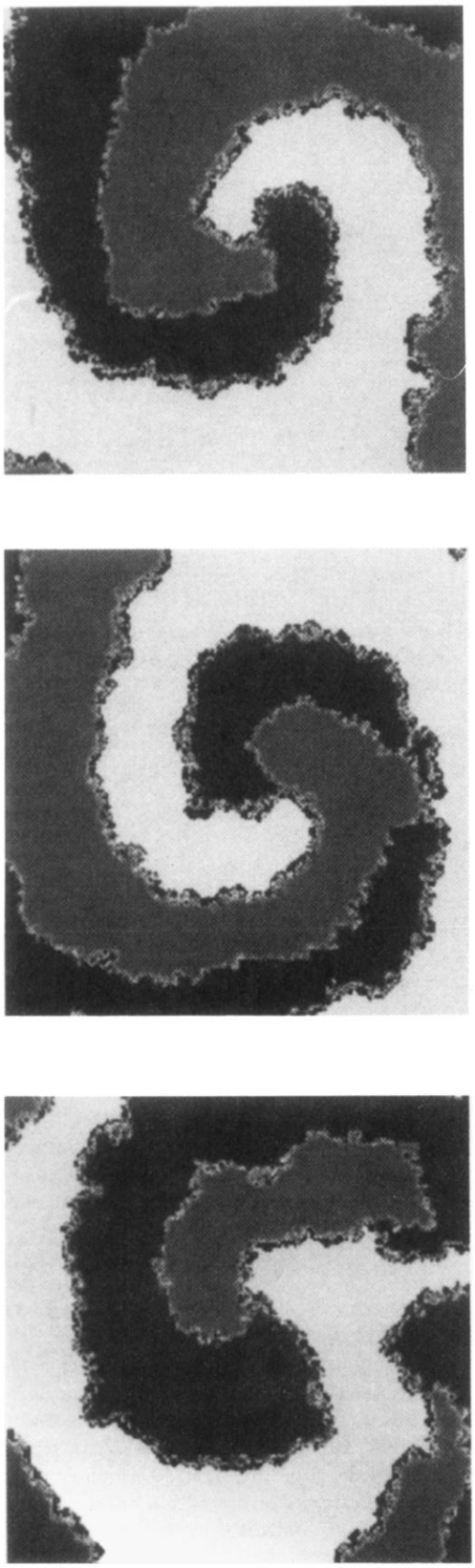

FIG. 15. Spiral wave dynamics and breakup initiated by the existence of a point defect where all three phases meet. The simulations were carried out on a 200×200 lattice with no-flux boundary conditions for $\varepsilon = 0.18$. From top to bottom, the frames are for $t = 2700$, $t = 3600$, and $t = 4500$, respectively.